Quantum scattering from arbitrary boundaries

M. G. E. da Luz,[1,*] A. S. Lupu-Sax,[1,†] and E. J. Heller[1,2,‡]
[1]*Department of Physics, Harvard University, Cambridge, Massachusetts 02138*
[2] *Harvard-Smithsonian Center for Astrophysics, Cambridge, Massachusetts 02138*
(Received 10 February 1997)

We present a conceptually and numerically simple method for obtaining scattering eigenstates from arbitrary disconnected open or closed boundaries with very general boundary conditions. As a side effect of the derivation, a solution for partially penetrable walls is also found. As in the boundary integral Green-function method, an integral equation over the boundary results; however, our approach uses δ-function potentials (which can have finite or infinite strength) to enforce boundary conditions and construct the governing equations, rather than Green's theorem. [S1063-651X(97)11308-3]

PACS number(s): 05.45.+b, 03.40.Kf, 03.65.Nk

I. INTRODUCTION

Much recent experimental and theoretical interest has been directed at boundary-value problems in two and three dimensions. Mesoscopic quantum dots and semiconductor heterostructures have become very important research tools and potentially useful devices. These are often accurately treated as billiard systems. Recently, quantum engineering experiments on metallic surfaces [1] have constructed quantum walls made of relatively few atoms. If the atoms are close enough together and some sorts of resonances [2] are avoided, one may build devices with nearly perfect walls as illustrated by ''quantum corrals'' [3]. Ordinary and superconducting thin microwave cavities have been constructed to address several issues involving quantum chaology and quantum localization; these are nearly exact quantum billiards. Of course, a solution to waveguide problems has been of great technological importance for decades.

This paper strikes out in a different direction than most theoretical treatments, arriving at an interesting (and accessible) approach to solving problems with sharp-walled boundaries, e.g., billiards, waveguides, and various compound objects including baffles, chambers, etc. While the discussion here focuses on the Schrödinger equation in two dimensions, the principles are applicable to other wave equations in two or more dimensions.

A nonrelativistic quantum-mechanical problem is solved only if one has a wave-function satisfying *both* the Schrödinger equation and the appropriate boundary conditions. The boundary conditions play an essential role in the system's dynamical behavior. For example, in billiard problems (free particles confined to finite regions of configuration space), wave-function properties (such as nodal patterns, ''scarring,'' etc.) and energy spectrum statistics, are quite different if the corresponding classical system is integrable (e.g., a circle or square) or chaotic (e.g., a Bunimovich stadium or Sinai billiard) [4].

Several approaches exist to finding scattering solutions to closed billiards, usually aimed at either the inside or outside solutions. A recent work has exploited connections between scattering problems and closed billiards [5]. Plane waves have been used as basis functions for matching the solutions at a boundary [6]. Perhaps the most popular method to solve boundary-value problems is the boundary integral method [7], which is based on the conversion of a differential equation into an integral over the boundary of the physical region. Although the boundary integral method is very useful, it has some drawbacks. Most notably, a boundary integral calculation is valid only on one side of a closed boundary [8], making it necessary to obtain different expressions for the solution inside and outside. It is also difficult to solve problems with disconnected and open boundaries.

It is desirable to have a method which (i) provides correct solutions on all sides of each boundary, (ii) gives solutions when a given asymptotic behavior is imposed away from the boundary, (iii) is simple and fast numerically, and (iv) is amenable to perturbation theory and other analytic approximations in ''small'' changes in the shape of the boundary [7].

Properties (i) and (ii) are intrinsic to scattering theory. However, scattering theory assumes that the boundary conditions are incorporated into the free Green function, while scattering takes place off of a potential. If we can create a potential which in an appropriate limit forces the wave function to satisfy the boundary conditions, we may use a scattering approach to the problem.

In this work we show that a ''δ-wall'' potential accomplishes this goal. Consider

$$V(\mathbf{r})=\int_{\mathcal{C}} ds\ \ \gamma(s)\,\delta(\mathbf{r}-\mathbf{r}(s))\{\alpha(s)-[1-\alpha(s)]\partial_{\mathbf{n}(s)}\}, \tag{1}$$

where the integral runs over the surface $\mathcal{C}$. The boundary condition [9]

$$\alpha(s)\psi(\mathbf{r}(s))|_{\mathcal{C}}+[1-\alpha(s)]\partial_{\mathbf{n}(s)}\psi(\mathbf{r}(s))|_{\mathcal{C}}=0 \tag{2}$$

then emerges as an appropriate limit of the potential's parameters ($\gamma\to\infty$). For finite γ, the potential has the effect of a penetrable or ''leaky'' wall. A similar idea has been used

*Electronic mail: luz@monsoon.harvard.edu
†Electronic mail: lupu-sax@typhoon.harvard.edu
‡Electronic mail: heller@physics.harvard.edu

 © 1997 The American Physical Society

to incorporate Dirichlet boundary conditions into certain classes of *solvable* potentials in the context of the path-integral formalism [10]. Here we use the δ wall more generally, resulting in a widely applicable and accurate procedure to solve boundary condition problems for arbitrary shapes.

This paper is organized as follows. In Sec. II we present the scattering theory approach for leaky and impenetrable Dirichlet walls. We solve two analytic examples in Sec. III. A numerical version of the method is given in Sec. IV, followed by some applications in Sec. V. The applications considered include numerical solutions of some open systems, an analysis of the quality of the numerical method, perturbation of boundaries, and closed billiard problems. We leave the derivations of the general boundary conditions (2) to Appendix B.

II. BOUNDARY WALL APPROACH

Consider the Schrödinger equation for a d-dimensional system, $H(\mathbf{r})\psi(\mathbf{r})=E\psi(\mathbf{r})$, with $H=H_0+V$. As is well known, the solution for $\psi(\mathbf{r})$ is given by

$$\psi(\mathbf{r})=\phi(\mathbf{r})+\int d\mathbf{r}'\,G_0^E(\mathbf{r},\mathbf{r}')V(\mathbf{r}')\psi(\mathbf{r}'), \tag{3}$$

where $\phi(\mathbf{r})$ solves $H_0(\mathbf{r})\phi(\mathbf{r})=E\phi(\mathbf{r})$, and $G_0^E(\mathbf{r},\mathbf{r}')$ is the Green function for H_0. Hereafter, for notational simplicity, we will suppress the superscript E in G_0^E.

Now we introduce a δ-type potential

$$V(\mathbf{r})=\gamma\int_{\mathcal{C}} ds\;\delta(\mathbf{r}-\mathbf{r}(s)), \tag{4}$$

where the integral is over $\mathcal{C}$, a connected or disconnected surface. $\mathbf{r}(s)$ is the vector position of the point s on $\mathcal{C}$ (we will call the set of all such vectors $\mathcal{S}$), and γ is the potential's strength. Clearly, $V(\mathbf{r})=0$ for $\mathbf{r}\notin\mathcal{S}$.

In the limit $\gamma\to\infty$, the wavefunction will satisfy Eq. (2) [with $\alpha(s)=1$] as shown below. In Appendix B we deal with more general boundary conditions and a potential strength $\gamma(s)$ which may vary over the curve. For finite γ, a wave function subject to potential (4) will satisfy a ''leaky'' form of the boundary condition as shown in Appendix A.

Inserting the potential (4) into Eq. (3), the volume integral is trivially performed with the δ function, yielding

$$\begin{aligned}\psi(\mathbf{r})&=\phi(\mathbf{r})+\gamma\int_{\mathcal{C}} ds'\,G_0(\mathbf{r},\mathbf{r}(s'))\psi(\mathbf{r}(s'))\\&=\phi(\mathbf{r})+\int_{\mathcal{C}} ds'\,G_0(\mathbf{r},\mathbf{r}(s'))T_\phi(\mathbf{r}(s')).\end{aligned} \tag{5}$$

Thus, if $\gamma\,\psi(\mathbf{r}(s))=T_\phi(\mathbf{r}(s))$ is known for all s, the wave function everywhere is obtained from Eq. (5) by a single quadrature. For $\mathbf{r}=\mathbf{r}(s'')$ some point of $\mathcal{S}$,

$$\psi(\mathbf{r}(s''))=\phi(\mathbf{r}(s''))+\gamma\int_{\mathcal{C}} ds'\,G_0(\mathbf{r}(s''),\mathbf{r}(s'))\psi(\mathbf{r}(s')), \tag{6}$$

which may be abbreviated unambiguously as

$$\psi(s'')=\phi(s'')+\gamma\int ds'\;G_0(s'',s')\;\psi(s'). \tag{7}$$

We can formally solve this equation, obtaining

$$\tilde{\psi}=[\tilde{I}-\gamma\,\tilde{G}_0]^{-1}\tilde{\phi}, \tag{8}$$

where $\tilde{\psi}$ and $\tilde{\phi}$ stand for the vectors of $\psi(s)$'s and $\phi(s)$'s on the boundary, and $\tilde{I}$ for the identity operator. The tildes remind us that the free Green-function operator and the wave vectors are evaluated only on the boundary.

We define

$$T=\gamma\,[\tilde{I}-\gamma\,\tilde{G}_0]^{-1}, \tag{9}$$

and then it is easy to see that T_ϕ in Eq. (5) is given from Eqs. (8) and (9) by

$$T_\phi(\mathbf{r}(s'))=\int ds\;T(s',s)\;\phi(s). \tag{10}$$

We can put Eq. (9) into another form by formally expanding in a power series

$$\gamma[\tilde{I}-\gamma\tilde{G}_0]^{-1}=\gamma\;\tilde{I}+\gamma\sum_{j=1}^{\infty}[\gamma\tilde{G}_0]^j. \tag{11}$$

In this way we find

$$T(s'',s')=\gamma\left(\delta(s''-s')+\sum_{j=1}^{\infty}T^{(j)}(s'',s')\right), \tag{12}$$

where

$$\begin{aligned}T^{(j)}(s'',s')=\gamma^j\int ds_1\ldots ds_j\;G_0(s'',s_j)\\\times G_0(s_j,s_{j-1})\;\ldots\;G_0(s_2,s_1)\;\delta(s_1-s').\end{aligned} \tag{13}$$

In order to make contact with the standard t-matrix formalism in scattering theory [11], we note that a T operator for the whole space may be written as

$$t(\mathbf{r}_f,\mathbf{r}_i)=\int ds''ds'\,\delta(\mathbf{r}_f-\mathbf{r}(s''))\;T(s'',s')\,\delta(\mathbf{r}_i-\mathbf{r}(s')). \tag{14}$$

Finally, we observe that Eq. (6) can be written as

$$\tilde{\psi}=[\tilde{I}+\tilde{G}_0T]\tilde{\phi}. \tag{15}$$

For $\gamma\to\infty$, the operator T converges to $-[\tilde{G}_0]^{-1}$. Inserting this into Eq. (15), we have

$$\tilde{\psi}=[\tilde{I}-\tilde{G}_0[\tilde{G}_0]^{-1}]\tilde{\phi}=0. \tag{16}$$

So, ψ satisfies a Dirichlet boundary condition on the surface $\mathcal{C}$ for $\gamma=\infty$.

III. ANALYTIC EXAMPLES

To illustrate the results of Sec. II, we explicitly analyze two two-dimensional systems below. We assume $H_0(\mathbf{r})=-\hbar^2/(2\mu)\nabla_{\mathbf{r}}^2$, the Hamiltonian for a free particle of mass μ. In this case $G_0(\mathbf{r},\mathbf{r}';k)=\sigma\, H_0^{(1)}(k|\mathbf{r}-\mathbf{r}'|)$, where $E=k^2\hbar^2/(2\mu)$, $\sigma=(2\mu/\hbar^2)(-i/4)$, and $H_0^{(1)}$ is the zero-order Hankel function of the first kind, which corresponds to outgoing spherical solutions of the free Schrödinger equation in two dimensions [12].

A. Free particle interacting with a circle

Consider $\mathcal{C}=\{(x,y)\in\mathbb{R}^2 \mid x^2+y^2=R^2\}$, parametrized by θ. From Eq. (13) we have the $T^{(j)}$'s given by ($\mathbf{u}(\theta'')=(R,\theta'')$, $\mathbf{u}(\theta')=(R,\theta')$)

$$T^{(1)}(\theta'',\theta')=\gamma\,\sigma\,H_0^{(1)}(k\sqrt{2}R\sqrt{1-\cos[\theta''-\theta']}), \tag{17}$$

and ($j=2,3,\ldots$)

$$\begin{aligned}T^{(j)}(\theta'',\theta')=(\gamma\sigma)^j\int_0^{2\pi}d\theta_2\ldots d\theta_j\\ \times H_0^{(1)}(k\sqrt{2}R\sqrt{1-\cos[\theta''-\theta_j]})\cdots\\ \times H_0^{(1)}(k\sqrt{2}R\sqrt{1-\cos[\theta_3-\theta_2]})\\ \times H_0^{(1)}(k\sqrt{2}R\sqrt{1-\cos[\theta_2-\theta']}).\end{aligned} \tag{18}$$

The integrals in Eq. (18) can be solved with the help of the identity (see Eq. 8.531 in Ref. [13]),

$$\begin{aligned}&H_0^{(1)}(k\sqrt{2}R\sqrt{1-\cos[\theta]})\\ &=J_0(kR)H_0^{(1)}(kR)+2\Sigma_{l=1}^{\infty}J_l(kR)H_l^{(1)}(kR)\cos[l\ \theta]\end{aligned}$$

(with J_l and $H_l^{(1)}$ the first kind l-order Bessel and Hankel functions, respectively), and also with the relation (l_1,l_2 integers) $\int_0^{2\pi}d\theta\cos[l_1(\theta-\theta')]\cos[l_2(\theta-\theta')]=2\pi$ if $l_1=l_2=0$ and $\pi\delta_{l_1l_2}\cos[l_1(\theta''-\theta')]$ otherwise. So, after tedious but straightforward calculations, one can show that ($j=1,2,3,\ldots$)

$$T^{(j)}(\theta'',\theta')=\frac{(\gamma 2\pi)^j}{2\pi}\left(F_0{}^j+2\sum_{l=1}^{\infty}F_l{}^j\cos[l(\theta''-\theta')]\right), \tag{19}$$

where $F_l=\sigma J_l(kR)H_l^{(1)}(kR)$. The full T matrix is obtained by putting Eq. (19) into Eq. (12). Since the sum over the $T^{(j)}$'s is a geometric series, the calculations can be performed exactly, and we find

$$\begin{aligned}T(\theta'',\theta')=\gamma\Bigg[\delta(\theta''-\theta')+\Bigg(\frac{\gamma F_0}{1-2\pi\gamma F_0}\\ +2\sum_{l=1}^{\infty}\frac{\gamma F_l}{1-2\pi\gamma F_l}\cos[l(\theta''-\theta')]\Bigg)\Bigg].\end{aligned} \tag{20}$$

As an application let us consider $\phi(\mathbf{r})=J_n(kr)\exp[in\theta]/\mathcal{N}$, with $\mathcal{N}$ a normalization constant. We have

$$\begin{aligned}T_\phi(\theta'')&=\gamma\int_0^{2\pi}d\theta'\Bigg(\delta(\theta''-\theta')+\frac{\gamma F_0}{1-2\pi\gamma F_0}\\ &\quad+2\sum_{l=1}^{\infty}\frac{\gamma F_l}{1-2\pi\gamma F_l}\cos[l(\theta''-\theta')]\Bigg)\\ &\quad\times\frac{1}{\mathcal{N}}J_n(kR)\exp[in\theta']\\ &=\frac{\gamma}{(1-2\pi\gamma F_n)}\frac{1}{\mathcal{N}}J_n(kR)\exp[in\theta'']. \end{aligned}\tag{21}$$

The wave function everywhere is given by Eq. (5), or

$$\psi(\mathbf{r})=\frac{1}{\mathcal{N}}\left(J_n(kr)+\frac{2\pi\gamma W_n(r)}{[1-2\pi\gamma F_n]}J_n(kR)\right)\exp[in\theta], \tag{22}$$

with

$$\begin{aligned}W_n(r)=1/(2\pi)\textstyle\int_0^{2\pi}d\theta''G_0(k\sqrt{r^2+R^2-2rR\cos[\theta'']})\\ \times\exp[in\theta'']\end{aligned}$$

.

This integral can be performed by again using Eq. 8.531 in Ref. [13], and one finds $W_n(r)=\sigma J_n(k\rho_<)H_n^{(1)}(k\rho_>)$, where $\rho_>$ ($\rho_<$) is the larger (smaller) between r and R. Note that $W_n(R)=F_n$. Thus Eq. (22) leads to

$$\psi(\mathbf{r})=\frac{1}{\mathcal{N}}\left(\frac{J_n(kr)}{1-2\pi\gamma\sigma J_n(kR)H_n^{(1)}(kR)}\right)\exp[in\theta]\quad\text{if } r<R \tag{23}$$

$$\psi(\mathbf{r})=\frac{1}{\mathcal{N}}\left(J_n(kr)+\frac{2\pi\gamma\sigma[J_n(kR)]^2H_n^{(1)}(kr)}{1-2\pi\gamma\sigma J_n(kR)H_n^{(1)}(kR)}\right)\times\exp[in\theta]\quad\text{if } r>R.$$

One can verify (for instance, by directly solving the Schrödinger equation) that Eq. (23) is the correct solution of a two-dimensional particle interacting with a radial δ function [14].

Now we consider the limit $\gamma\to+\infty$. We denote the radial part of $\psi(\mathbf{r})$ by $f_\gamma(r)$ and we have the following: (i) For $r<R$, $f_\infty(r)$ is different from zero only if $kR=\alpha_{nm}$, where α_{nm} is the mth root of J_n. In this case $f_\infty(r)=J_n(\alpha_{nm}r/R)$, the correct solution for a particle confined in a circle. (ii) For $r>R$, $f_\infty(r)=i[J_n(kr)Y_n(kR)-J_n(kR)Y_n(kr)]/H_n^{(1)}(kR)$, with Y_n the n-order Bessel function of second kind (Neumann function). Once more we get the exact solution, this time for a free particle outside an impenetrable circular wall.

B. Free particle interacting with an infinite line

Often one may be interested only in a particular kind of incoming wave $\phi(\mathbf{r})$. In this case it is not necessary to cal-

culate T, but just T_ϕ. Here we show a direct calculation of T_ϕ for $\mathcal{C}$ the line $x=0$ (parametrized by y) and $\phi(\mathbf{r}) = \exp[i(k_x x + k_y y)]/\mathcal{N}$, with $k^2 = k_x^2 + k_y^2$, and $\mathcal{N}$ an appropriate normalization constant. We also assume $k_x > 0$, i.e., ϕ is incoming from the left (in the x direction).

Putting Eq. (12) into Eq. (10), we can easily show that $[\mathbf{r}(y) = (0,y)]$

$$T_\phi(y) = \frac{1}{\mathcal{N}} \exp[ik_y y] \sum_{j=0}^{\infty} [\gamma I(0)]^j = \frac{1}{\mathcal{N}} \exp[ik_y y] \frac{1}{[1-\gamma I(0)]}, \tag{24}$$

where $I(z) = \sigma \int_{-\infty}^{+\infty} dy\ H_0^{(1)}(k\sqrt{y^2+z^2})\ \exp[ik_y y]$.

By inserting Eq. (24) into Eq. (5), we have

$$\psi(\mathbf{r}) = \frac{1}{\mathcal{N}} \exp[ik_y y] \left(\exp[ik_x x] + \frac{\gamma I(x)}{1-\gamma I(0)} \right). \tag{25}$$

The integral I is solved with the help of identity Eq. 6.616-3 in Ref. [13], or

$$I(x) = \frac{\mu}{i\hbar^2 k_x} \exp[ik_x |x|]. \tag{26}$$

Defining $\zeta = (\gamma\mu)/(i\hbar^2 k_x)$, $\mathcal{T}(k_x) = 1/(1-\zeta)$, and $\mathcal{R}(k_x) = \zeta/(1-\zeta)$, we finally find

$$\psi(\mathbf{r}) = \frac{1}{\mathcal{N}} \exp[ik_y y] \times \begin{cases} (\exp[ik_x x] + \mathcal{R}(k_x)\exp[-ik_x x]) & \text{if } x<0 \\ \mathcal{T}(k_x)\exp[ik_x x] & \text{if } x>0. \end{cases} \tag{27}$$

We observe that the infinite line is a separable system. Thus the solution of the Schrödinger equation is a plane wave in the y direction times the solution of a one-dimensional δ function in the x direction. Actually, one can verify that Eq. (27) is exactly in this form, therefore we have obtained the correct wave function for the problem. If we take the limit $\gamma \to +\infty$, the line becomes an infinite wall, and ψ should be zero for $x \geqslant 0$ (recall that the incident wave comes from the left). Indeed, this is the result we obtain from Eq. (27).

IV. *T* MATRIX: A NUMERICAL TREATMENT

As discussed in Sec. II and illustrated in Sec. III, the key idea in our method is to calculate T and/or T_ϕ on $\mathcal{C}$, and then to perform integral (5). Unfortunately, in the great majority of cases the analytical treatment is too hard to apply. In such cases we consider the problem numerically.

We divide the region $\mathcal{C}$ into N parts, $\{\mathcal{C}_j\}_{j=1\ldots N}$. Then we approximate

$$\psi(\mathbf{r}) = \phi(\mathbf{r}) + \sum_{j=1}^{N} \int_{\mathcal{C}_j} ds\ \gamma\ G_0(\mathbf{r},\mathbf{r}(s))\ \psi(\mathbf{r}(s)) \approx \phi(\mathbf{r}) + \sum_{j=1}^{N} \int_{\mathcal{C}_j} ds\ \gamma\ G_0(\mathbf{r},\mathbf{r}(s))\ \psi(\mathbf{r}(s_j)), \tag{28}$$

with s_j the middle point of $\mathcal{C}_j$ and $\mathbf{r}_j = \mathbf{r}(s_j)$. Now, considering $\mathbf{r} = \mathbf{r}_i$ we write $\psi(\mathbf{r}_i) = \phi(\mathbf{r}_i) + \sum_{j=1}^{N} \gamma\ M_{ij}\psi(\mathbf{r}_j)$ (for M, see discussion below). If $\Psi = (\psi(\mathbf{r}_1), \ldots, \psi(\mathbf{r}_N))$, and $\Phi = (\phi(\mathbf{r}_1), \ldots, \phi(\mathbf{r}_N))$, we have $\Psi = \Phi + \gamma\mathbf{M}\Psi$, and thus $\gamma\Psi = \mathbf{T}\Phi$, with $\mathbf{T} = \gamma(\mathbf{I} - \gamma\mathbf{M})^{-1}$, which is the discrete T matrix. So

$$\gamma\Psi_i = (\mathbf{T}\Phi)_i = \gamma \sum_{j=1}^{N} [(\mathbf{I} - \gamma\mathbf{M})^{-1}]_{ij}\Phi_j \tag{29}$$

and

$$\psi(\mathbf{r}) \approx \phi(\mathbf{r}) + \sum_{j=1}^{N} G_0(\mathbf{r},\mathbf{r}_j)\ \Delta_j\ (\mathbf{T}\Phi)_j, \tag{30}$$

where we have used a mean value approximation to the last integral in Eq. (28), and defined Δ_j, the volume of $\mathcal{C}_j$.

It follows from Eq. (28) that

$$M_{ij} = \int_{\mathcal{C}_j} ds\ G_0(\mathbf{r}_i, \mathbf{r}(s)). \tag{31}$$

Unless otherwise mentioned, we will approximate

$$M_{ij} \approx G_0(\mathbf{r}_i, \mathbf{r}_j)\ \Delta_j \tag{32}$$

in our example calculations. However, $G_0(\mathbf{r}_i, \mathbf{r}_j)$ may diverge for $i=j$ (e.g., the free-particle Green functions in two or more dimensions). So, for the diagonal terms M_{ii} we explicitly perform integral (31). We discuss these approximations in detail in Sec. V B.

If we consider $\gamma \to \infty$, it is easy to show from the above results that

$$\psi(\mathbf{r}) \approx \phi(\mathbf{r}) - \sum_{j=1}^{N} G_0(\mathbf{r},\mathbf{r}_j)\Delta_j\ (\mathbf{M}^{-1}\Phi)_j. \tag{33}$$

Equation (33) is then the approximated wave function of a particle under H_0 interacting with an impenetrable region $\mathcal{C}$.

V. APPLICATIONS

Here we shall to explore the possibilities of applications for the method described in previous Sec. IV. We concentrate on two-dimensional systems and assume $\gamma \to \infty$, which corresponds to Dirichlet boundary conditions for the wave function on $\mathcal{C}$. Thus from now on the calculations are done by using Eq. (33), where we consider only sets $\{\mathcal{C}_j\}$ such that $\Delta_j = \Delta$ a constant (all the curves $\mathcal{C}_j$ have the same total length Δ). For the plots of $|\psi(x,y)|^2$ we take a grid of 400×400 points in the x-y plane. Since, for our purposes, we are only concerned with relative amplitudes, in each region considered we normalize the maximum value of $|\psi|^2$ (or ψ in Sec. V D) to be 1. For simplicity, $\hbar = 2\mu = 1$, so $E = k^2$.

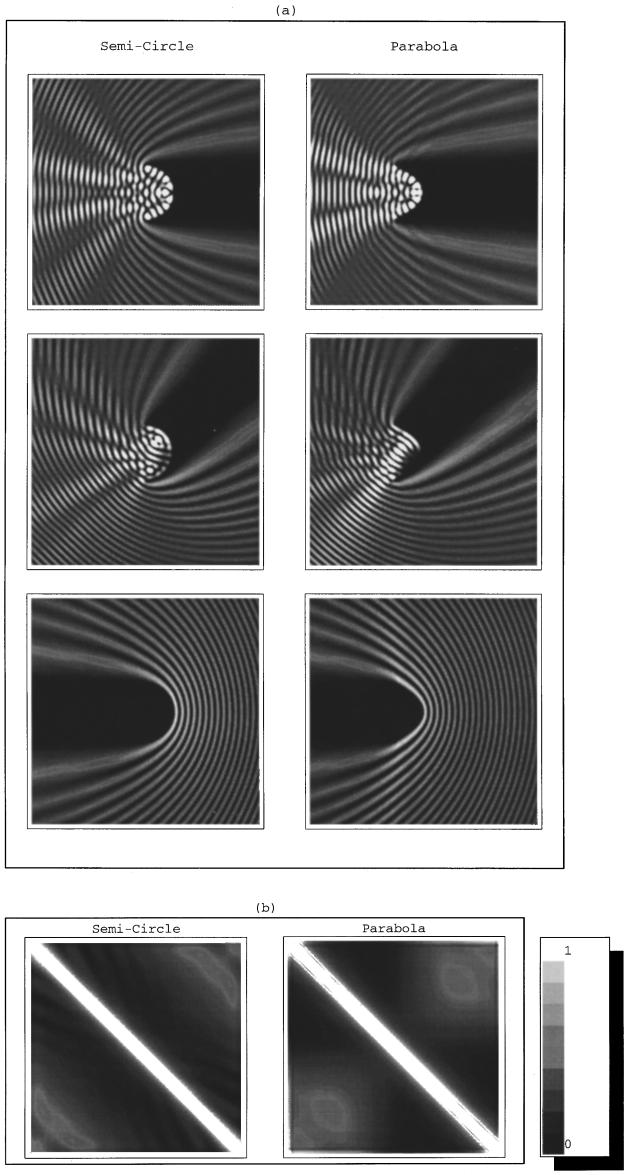

FIG. 1. (a) Scattering of plane waves by a semicircle and a segment of the parabola. (b) Density plots of $|T|$ for the semicircle and the segment of the parabola in (a). The gray scale is valid for all plots of $|\psi|^2$ and $|T|$ in this paper.

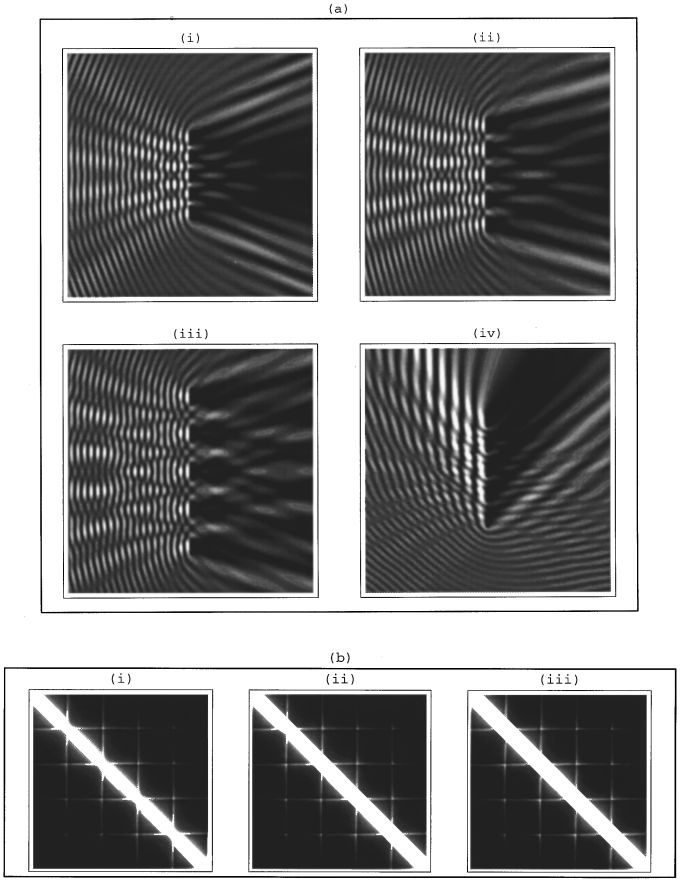

FIG. 2. Scattering of plane waves by diffraction nets. (b) Density plots of $|T|$ for the diffraction nets in (a). The diffraction effects are readily identified in the $|T|$ matrix as the bright patterns off the main diagonal.

A. Open $\mathcal{C}$'s

Figures 1–3 show a sample of different open forms for $\mathcal{C}$. In Figs. 1–3(a) we plot $|\psi|^2$. Density plots of the modulus of the corresponding matrix elements $|T_{ij}|$ are presented in Figs. 1–3 (b). We used 200 (400) points on the $\mathcal{C}$'s for Figs. 1 and 2 (3). Thus T was obtained by inverting a 200×200 (400×400) matrix. Here we should note that (i) by construction the T's are symmetric matrices; and (ii) in general, the larger $|T_{ij}|$'s are those from a band around the main diagonal, as one can see in the figures.

In Fig. 1(a) we show the scattering of a plane wave by the semicircle $x^2+y^2=1$ $(x\geqslant0)$, and by the segment of parabola $x=-y^2$ $(-1\leqslant y\leqslant1)$. The wavelength $\lambda=2\pi/k$ is $2\pi/15\approx0.42$. In both cases we consider three different angles between the wave vector of the incoming wave and the x axis: 0°, 45°, and 180°.

Figure 2(a) shows a diffraction net formed by five segments of line along $y=0$. Each has length 0.4 and is separated from the next by a distance of (i) 0.21, (ii) 0.42, (iii) 0.84, and (iv) 0.42. For the incident plane wave $\lambda=2\pi/15\approx0.42$, with the wave vector forming angles of 0° [(i)–(iii)], and 30° [(iv)], with the x axis.

In Fig. 3(a) we consider two semicircles (represented in the top left graphic). The ϕ's are $\phi(\mathbf{r})=\exp[ikx]$, and $\phi(\mathbf{r})=J_0(k|\mathbf{r}-\mathbf{r}_c|)$ [with $\mathbf{r}_c$ being (0,0) and (3.5,3.5)]. For the three, $k=20$ ($\lambda\approx0.31$), so the T matrix displayed in Fig. 3(b) is the same in all cases.

B. Performance of the numerical method

The numerical solution (33) approaches the solution (5) as $N\to\infty$. In practice, we choose N to be some finite but large number. In this section we explain how to choose N for a given problem, and how the approximation (32) affects this choice.

In order to analyze the performance of the numerical solution, we must define some measure of the quality of the solution. We measure how well a Dirichlet boundary blocks the flow of current directed at it. Thus we measure the current

$$\mathbf{j}=\mathrm{Im}\{\psi^*(\mathbf{r})\nabla\psi(\mathbf{r})\}, \tag{34}$$

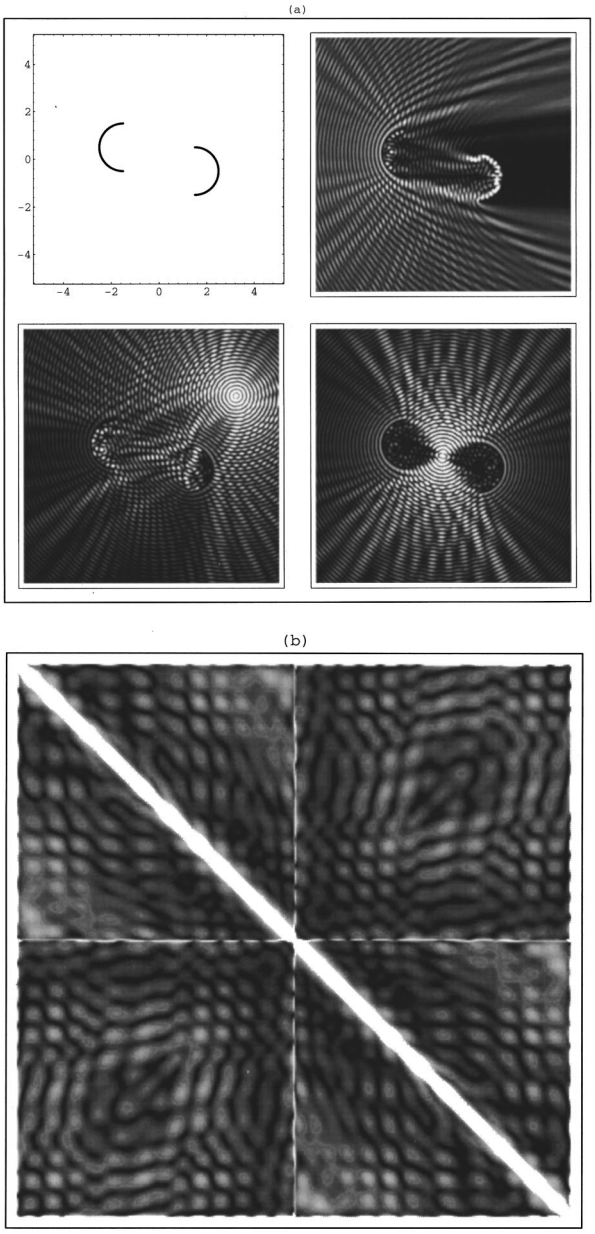

FIG. 3. Scattering by the two semicircles represented in the top left graphic. The incoming ϕ's are (top right) a plane-wave function and (bottom) a Bessel function J_0. (b) Density plot of $|T|$ for the two semicircles in (a). It is interesting to note the much richer structure of the T matrix for the two semicircles in comparison with the T matrix for the single semicircle in Fig. 1(b).

behind a straight wall of length l. To simplify the analysis we integrate $\mathbf{j}\cdot\mathbf{n}$ over a ''detector'' located on one side of a wall with a normally incident plane wave on the other side. We divide this integrated current by the current which would have been incident on the detector without the wall present. We call this ratio $\mathcal{T}$ the transmission coefficient of the wall. Instead of $\mathcal{T}$ as a function of N, we consider $\mathcal{T}$ vs ρ, where $\rho=2\pi N/(lk)$ is the number of boundary pieces per wavelength.

We consider three methods of constructing the matrix $\mathbf{M}$ for each value of ρ. The first is the approximation used in the applications in this paper (where typically $\rho\approx 40$)

$$M_{ij}=\begin{cases}\displaystyle\int_{\mathcal{C}_i} ds\ G_0(\mathbf{r}_i,\mathbf{r}(s)), & i=j\\ \Delta G_0(\mathbf{r}_i,\mathbf{r}_j), & i\neq j,\end{cases} \tag{35}$$

which we call the ''fully approximated'' $\mathbf{M}$. The next is a more sophisticated approximation with

$$M_{ij}=\begin{cases}\displaystyle\int_{\mathcal{C}_j} ds\ G_0(\mathbf{r}_i,\mathbf{r}(s)), & |s_i-s_j|<\dfrac{\kappa}{k}\\ \Delta G_0(\mathbf{r}_i,\mathbf{r}_j), & |s_i-s_j|\geqslant\dfrac{\kappa}{k},\end{cases} \tag{36}$$

which we call the ''band-integrated'' $\mathbf{M}$ because we perform the integrals only inside a band of $\kappa/(2\pi)$ wavelengths. Finally, we consider

$$M_{ij}=\int_{\mathcal{C}_j} ds\ G_0(\mathbf{r}_i,\mathbf{r}(s))\quad \forall ij, \tag{37}$$

which we call the ''integrated'' $\mathbf{M}$.

Numerically, the ''band-integrated'' and ''integrated'' $\mathbf{M}$ require far more computational work than the ''fully approximated'' $\mathbf{M}$ which requires the fewest integrals. All methods of calculating $\mathbf{M}$ scale as $O(N^2)$. The calculation of $\mathbf{T}$ or $\mathbf{T}\Phi$ from $\mathbf{M}$ scales as $O(N^3)$ and the calculation of $\psi(\mathbf{r})$ for a particular $\mathbf{r}$ from a given $\mathbf{T}\Phi$ scales as $O(N)$. Which of these various calculations dominates the computation time depends on what sort of computation is being performed. When computing wave functions, computation time is typically dominated by the large number of $O(N)$ vector multiplications. However, when calculating $\psi(\mathbf{r})$ in only a small number of places, e.g., when performing a flux calculation, computation time is often dominated by the $O(N^3)$ construction of $\mathbf{T}\Phi$.

In Fig. 4 we plot $\log_{10}\mathcal{T}$ vs ρ for the three methods above and $2\leqslant\rho\leqslant 30$. We see that all three methods block more than 99% of the current for $\rho>5$. However, it is clear from the figure that the ''integrated'' $\mathbf{M}$ and to a lesser extent the band integrated $\mathbf{M}$ strongly outperform the fully approximated $\mathbf{M}$ for all ρ plotted.

C. Perturbation theory

One can use perturbative methods to solve $\mathcal{C}$'s of similar shapes. Consider two curves, $\mathcal{C}^B$ and $\mathcal{C}^A$, of same total length [15], as displayed in Fig. 5. It is not difficult to write down a formal expression relating their T matrices. A bit of algebra shows [with the help of Eqs. (9) and (11)]

$$T^B=T^A[I-\Gamma\ T^A]^{-1}=T^A(I+\Gamma\ T^A+\Gamma\ T^A\ \Gamma\ T^A+\cdots), \tag{38}$$

where

$$\begin{aligned}\Gamma(s'',s')&=G_0^B(s'',s')-G_0^A(s'',s')\\ &=G_0(\mathbf{r}^B(s''),\mathbf{r}^B(s'))-G_0(\mathbf{r}^A(s''),\mathbf{r}^A(s')),\end{aligned} \tag{39}$$

with $\mathbf{r}^B(s)$ and $\mathbf{r}^A(s)$, respectively, the vector positions of the point s on $\mathcal{C}^B$ and $\mathcal{C}^A$. If the $\mathcal{C}$'s are similar, Γ is small and we may truncate Eq. (38) at some order in Γ. Although, for

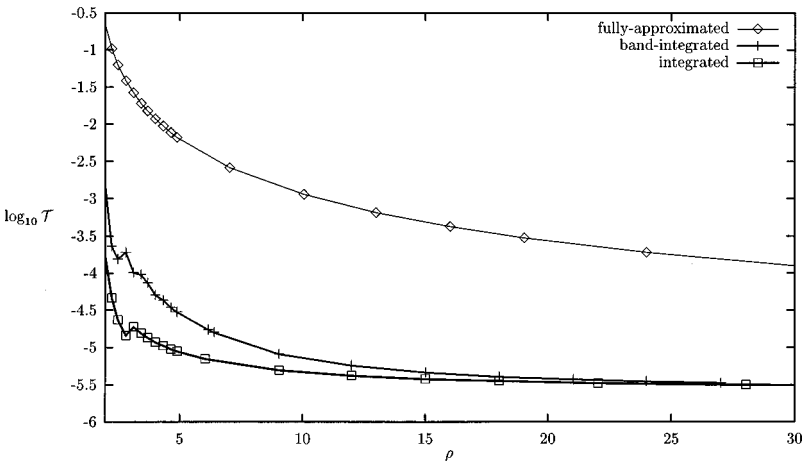

FIG. 4. Transmission of a finite flat wall for the various approximations of **M**. For the ''band-integrated'' method, $\kappa = 16\pi$.

the purposes of the present work, we are not going to develop the above equations any further, we will, for a particular example, study Eq. (38) in its simplest form, i.e., by taking the zero-order approximation $T^B \approx T^A$.

In Fig. 6 we have the curve $x=(l/2)\sin[4\pi y]$ $(0 \leqslant y \leqslant \pi/2)$ and an incident plane wave $\phi(\mathbf{r})=\exp[ikx]$, $k=15$. We plot in Fig. 6(a) $|\psi|^2$ calculated by using in Eq. (33) (i) the correct (numerical) T, and (ii) the (numerical) T for a straight line of same total length as the sinelike curve considered. In all cases we take 200 points on $\mathcal{C}$ to obtain the T matrix. The values of l are $l=0.1$, 0.3, 0.5, and 0.7. For a better comparison, we plot in Fig. 6(b) $|\psi(x,y)|^2$ (for fixed y's) as function of x. We see that the solutions using the T matrix for a straight line, when compared with those of correct T, are good for $l = 0.1$ and 0.3, intermediate for $l = 0.5$, and worst for $l=0.7$. These results are not due to the particular shape assumed for $\mathcal{C}$. We have done this same kind of analysis for other shapes and found that for small deformations of the curves, one can obtain good results by just considering the zeroth-order perturbative expansion of every other T matrix.

D. Closed $\mathcal{C}$'s: billiard problems

A last point we shall discuss is $\mathcal{C}$ as a closed curve, with its inside region being then a billiard. In this case our procedure provides a scattering approach for the quantization of the system, which is, however, different from other scattering methods [16].

The idea is straightforward. We have an incident wave function ϕ of energy E. If E is not a resonance energy of the billiard, ψ is the appropriate scattering solution outside $\mathcal{C}$ and zero inside. But if E is an eigenenergy of the problem, then ψ should be, inside the billiard, a linear combination of the eigenfunctions corresponding to that particular energy.

To verify this, we suppose a two-dimensional square box [with corners located at (0,0), (0,1), (1,1) and (1,0)]. The quantized energies are $\pi^2(n^2+m^2)$ $(n,m=1,2,\ldots)$, with the wave functions (up to a normalization constant) $\sin[n\pi x]\sin[m\pi y]$. For the incoming waves we consider $\phi(\mathbf{r})=\exp[i(k_x x+k_y y)]$, with $k_x=k\cos[\theta]$ and $k_y=k\sin[\theta]$ $(E=k^2)$. In the numerical calculations of the T matrix, $N=200$.

In Fig. 7(a) we have $\theta=\pi/4$ $(k_x=k_y)$ and (i) $k=0.997\sqrt{2}\pi$, (ii) $k=1.001\sqrt{2}\pi$, and (iii) $k=1.004\sqrt{2}\pi$. The exact ground-state energy of the box corresponds to $k=\sqrt{2}\pi$. From the plots of $|\psi|^2$ in (i) and (iii) we see that the wave function inside the square is quite small. To give an order of magnitude, the maximum of $|\psi|^2$ inside the box is about 40 times smaller than the maximum of $|\psi|^2$ outside [see the plot of $|\psi(x,\frac{1}{2})|^2$ against x for these two cases]. If we go further away from the resonance energy, the ψ within the box practically vanishes. That is, the resonances are very sharp in energy. For example, if we assume the resonance width ΔE to be the difference between the energies of (iii) and (i), then ΔE is just 1% of the correct ground-state energy.

The maximum amplitudes for ψ within $\mathcal{C}$ is reached at $k=1.001\sqrt{2}\pi$, an error of only 0.2%. In the density plot in (ii), the amplitudes inside the square are so much higher than the scattering wave outside (around 50 times) that to obtain some contrast we have plotted $\log_{10}|\psi|^2$ instead of $|\psi|^2$. We also compare $|\psi(x,1/2)|^2$ calculated numerically (solid line) with the exact solution $|\sin(\pi x)\sin(\pi/2)|^2$ (dashed line). We almost cannot distinguish between the two. By using larger T matrices, one can narrow ΔE as well improve the values for the resonance energy.

We may consider the effect of changing the direction of the incident wave. For the calculations of the ground state above, different choices for θ give the same sort of results displayed in Fig. 7(a), even for the cases of $\theta=0$ and $\theta=\pi/2$. However, there is an angular dependence when we consider degenerate states. For instance, for $E=50\pi^2$, the three incident wave vectors $\theta \approx 8.13°$ $(k_x=7\pi, k_y=\pi)$, $\theta=45°$ $(k_x=5\pi, k_y=5\pi)$, and $\theta \approx 81.87°$ $(k_x=\pi, k_y=7\pi)$ correspond, respectively, to the eigenstates: $n=7, m=1$;

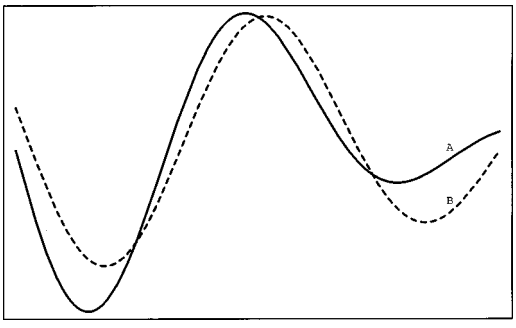

FIG. 5. Two curves $\mathcal{C}^A$ and $\mathcal{C}^B$ of the same total length.

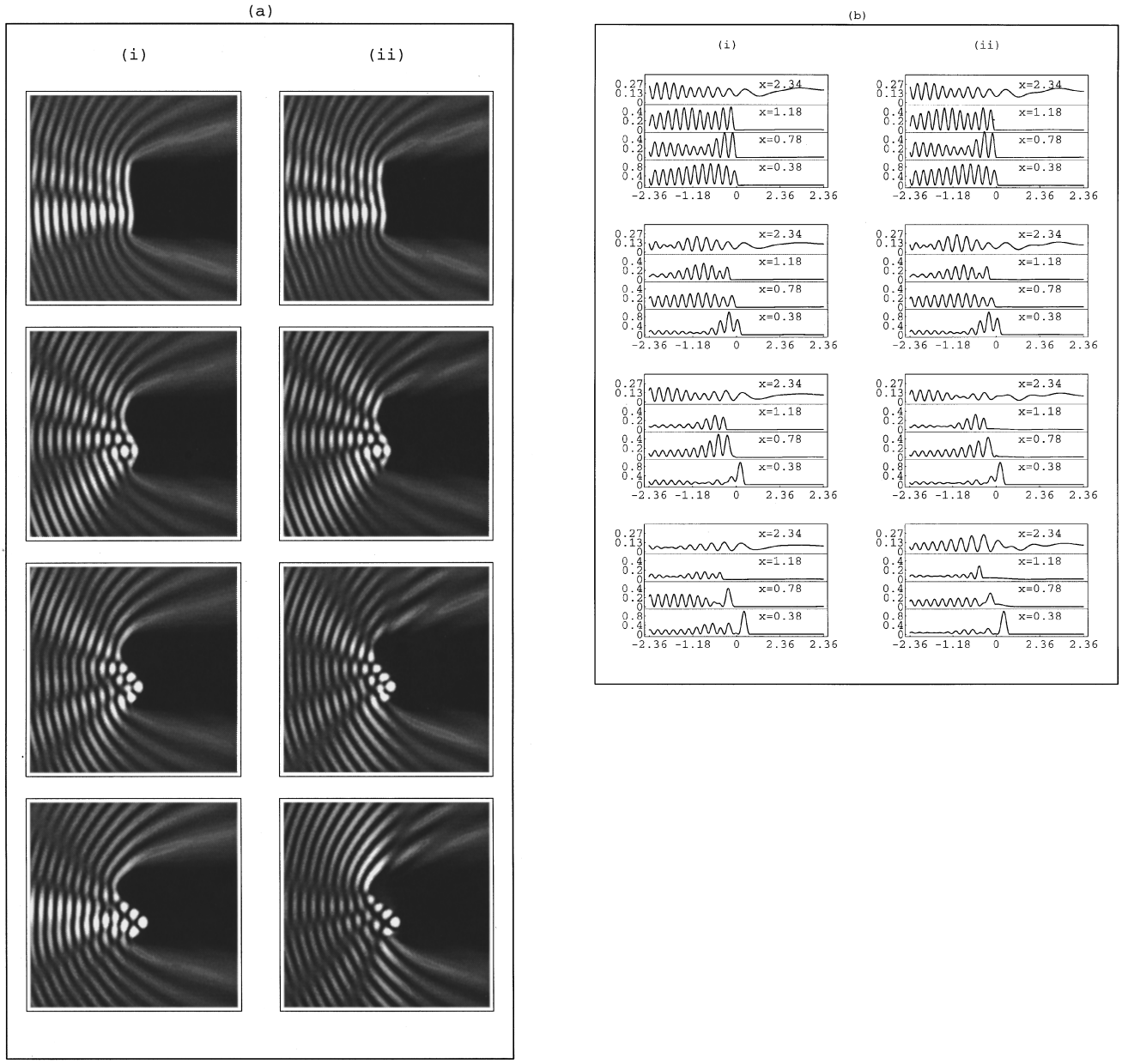

FIG. 6. (a) Scattering of the plane waves by sinelike shapes calculated with (i) the correct T matrix and (ii) the T matrix for a straight line. (b) Same as (a), but now for $|\psi(x,y)|^2$ as a function of x for some fixed values of y.

$n=5,m=5$; and $n=1,m=7$. When the incident plane wave, with the correct resonant wave number k (which in our calculations is around 0.1% off the exact value $\sqrt{50}\pi$), has one of the above three directions, then only that particular eigenstate is excited. For arbitrary directions, ψ is a linear combination of the degenerate states.

In Fig. 7(b) we show the plot of the ψ for (i) $\theta\approx 81.87°$, (ii) $\theta=45°$, and (iii) $\theta\approx 26.56°$. (i) and (ii) agree very well with their corresponding single eigenstates. For (iii), we find that the coefficients $c_{n,m}$ of the linear combination are $c_{1,7}=4.317$, $c_{5,5}=-7.096$, and $c_{7,1}=-1$ (we have set $c_{7,1}=-1$ and normalized the other two in terms of it). We also compare $\psi(\frac{1}{2},y)$ from our calculations (continuous line) with the exact (dashed line) for all cases. A theory explaining how the c's depend on θ will be the subject of a future contribution.

Finally, we briefly give an example of resonance for an open curve $\mathcal{C}$. Consider two semicircles separated by a distance d, as schematically represented in Fig. 8. The incoming wave is $\phi(\mathbf{r})=\exp[ikx]$, with $k=10$. For the T matrix we take 400 points on $\mathcal{C}$. Varying d we can have pattern formations within the semicircle region. In detail we plot $|\psi(x,0.53)|^2$ for two very close values of d, which shows the dramatic difference of amplitudes of ψ in and out of the semicircle region according to whether or not we are in resonance.

VI. CONCLUSIONS AND PROSPECTS

The scattering T matrix which we calculate in this paper is an object intrinsic to the shape of the walls and the energy; it takes any incoming condition $\phi(\mathbf{r})$ and turns it into a solution which vanishes on the walls (or satisfies other

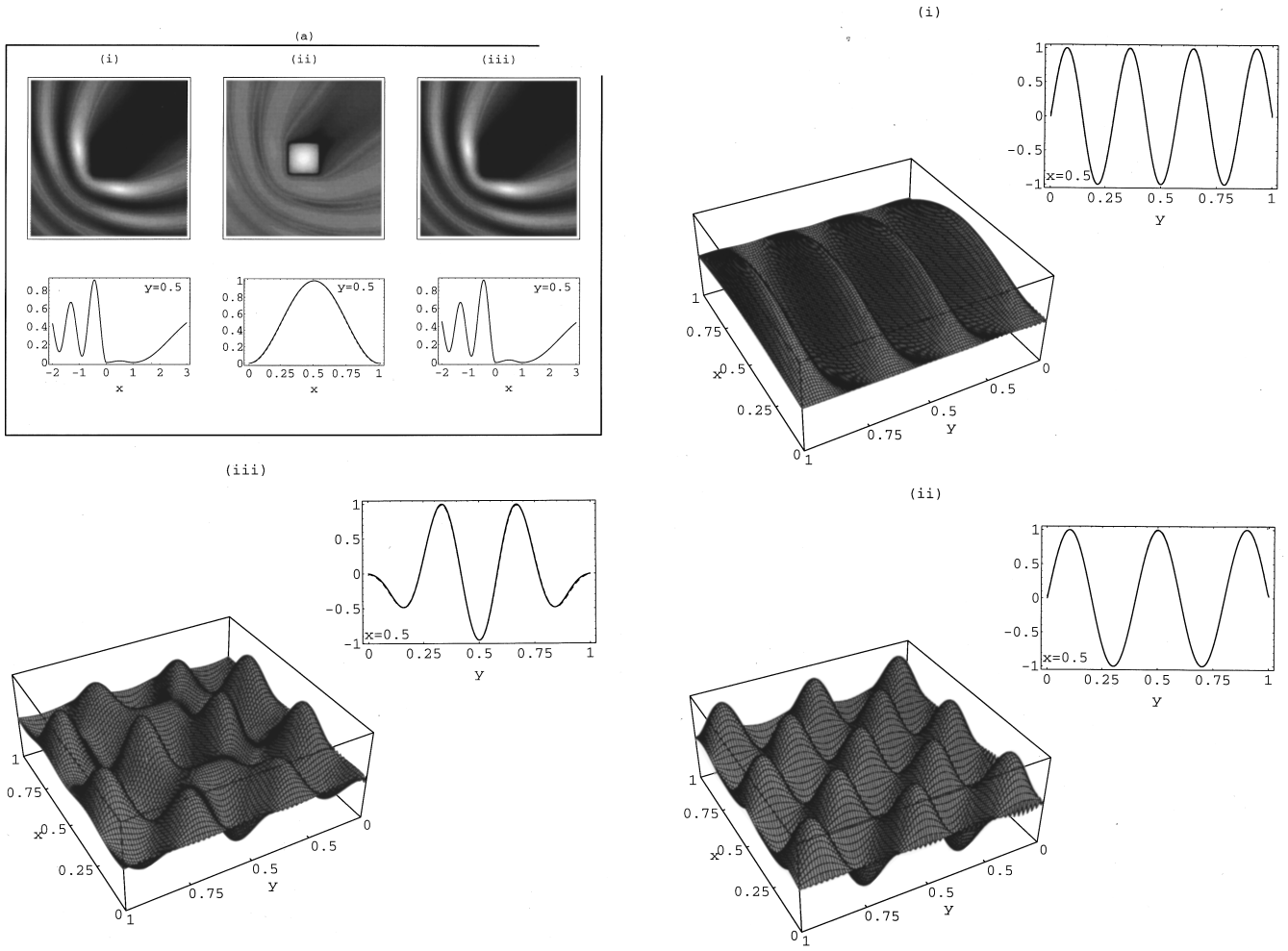

FIG. 7. (a) Scattering of plane waves by a square billiard for three different values of k. (b) Plots of the scattering excited ψ inside the square billiard for three different angles of the incident wave vectors. In detail we compare the exact (continuous line) and numerical (dashed line) $\psi(0.5,y)$'s as functions of y.

boundary condition there; see Appendix B). It also has a very appealing physical interpretation: referring to Eqs. (14), (5), and (10), we see that the element $T(s'',s')$ is the amplitude for hitting the walls for the first time at $\mathbf{r}(s')$ and for the last time at $\mathbf{r}(s'')$. All intermediate multiple collisions with different parts of the wall are included in $T(s'',s')$. After a discretization and inversion of the boundary Green function to obtain $T_{ij}=T(s_i,s_j)$, inspection of the structure of T_{ij} reveals the following general properties: (1) $|T_{ij}|$ is large for $|\mathbf{r}(s_i)-\mathbf{r}(s_j)|\leqslant\lambda(E)$, where $\lambda(E)$ is the wavelength at energy E; (2) sharp corners and wall ends tend to give brighter rows and columns in the density plots of T [see Figs. 1–3(b)], corresponding to higher amplitude for starting or leaving from such sources of diffraction; and (3) other bands in $|T_{ij}|$ reveal scattering between distinct or disjoint sections of walls that are reached by travel through space.

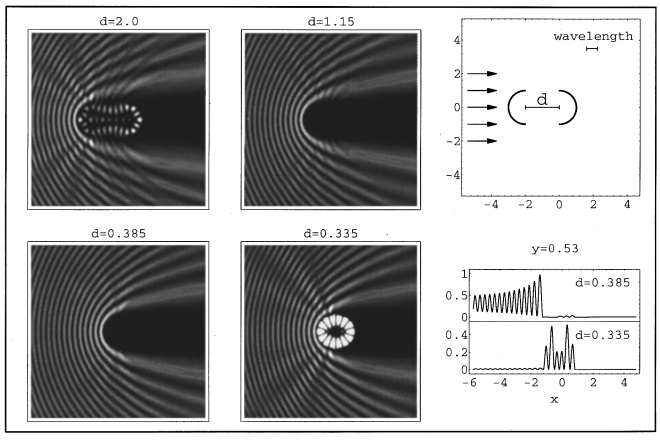

FIG. 8. Scattering of plane waves by two semicircles for different distances d between them.

We make two points regarding the case of closed $\mathcal{C}$'s. First, we have seen from the square billiard example that the resonances are very narrow, and the method gives very good results for the eigenstates. The computational time necessary in scanning k to find the correct resonances is common to all boundary methods, and is the ''price paid'' for the efficiency of working in the reduced space of the boundary only.

The second point concerns the question: what is the most appropriate φ to find the bound states? Except for degeneracies, the bound-state wave function dominates near the bound-state energies, and one can be fairly loose about the

precise nature of φ. In the case of degeneracy induced by symmetry, the incoming wave will excite a particular linear combination: one should of course choose the incoming wave with the desired symmetry. For example, for the square billiard in Sec. V, for $k=\pi\sqrt{5}$, by choosing $\theta=\arctan[1/2]$ ($\theta=\pi/2-\arctan[1/2]$) one obtains the state $n=2$, $m=1$ ($n=1$, $m=2$). However, we do not need to know these ''magic angles'' to excite just one state. If we consider $\varphi(\mathbf{r})=\exp[i\pi\sqrt{5}x]$, the only bound state we can obtain is $n=2$, $m=1$, because φ is symmetric along the y axis but the state $n=1$, $m=2$ is antisymmetric about $y=\frac{1}{2}$! Actually, this same idea would works for other shapes, say, for the stadium billiard.

Although error analysis of the δ wall approach is still under investigation, we find the following: (1) relatively crude midpoint quadrature approximations to the integral equations to give a discrete, numerical version of the problem give results which are quite useful for many purposes; (2) sensitive tests, such as measurements in ''dark,'' classically forbidden zones or fluxes through narrow slits require more care, but careful quadratures are rewarded with orders of magnitude increase in accuracy; (3) from Eq. (33) we see that $\psi(\mathbf{r})$ properly vanishes on $\mathcal{C}$ at the points $\mathbf{r}_i$'s [observe that, if $\mathbf{r}=\mathbf{r}_i$, in Eq. (33) we make the natural substitution of $G_0(\mathbf{r}=\mathbf{r}_i,\mathbf{r}_j)\Delta_j$ with M_{ij}]. A good verification for the method is then to calculate the wave function in other points on the boundary, for instance at the intermediate points $\overline{s_i}$, i.e., in the middle of s_i and s_{i+1}. In doing so, for the typical values of k and N used in this paper for open and closed shapes, we found that on average $|\psi(\overline{s_i})|^2$ is of the order of 10^{-4}. We also noticed that by increasing N the values of $|\psi(\overline{s_i})|^2$ decrease.

The method is currently being used to investigate the properties of mesoscopic semiconductor heterostructures. It is hoped that more progress can be made using the structure of the T matrix to understand diffraction, semiclassical limit approximations, and multiple-scattering expansions.

ACKNOWLEDGMENTS

M.G.E. da L. is supported by CNPq (Brazil) and A.S.L.-S. by the National Science Foundation graduate research fellowship program. This work was supported by the National Science Foundation under Grant No. CHE-9321260.

APPENDIX A: LEAKY BOUNDARIES

To clarify the physical meaning of γ in Eq. (4) [which here may be a function of position, $\gamma(s)$], we consider the two-dimensional case, with $\mathcal{C}$ an arbitrary curve (see Fig. 9). Also, to simplify our discussion, we decompose the unperturbed (incoming) wave as $\phi(\mathbf{r})=\int d^2k\, c(\mathbf{k})\phi_{\mathbf{k}}(\mathbf{r})$, where $\phi_{\mathbf{k}}(\mathbf{r})=(2\pi)^{-1}\exp[i\mathbf{k}\cdot\mathbf{r}]$, and focus on each $\phi_{\mathbf{k}}$.

For a particular point s on $\mathcal{C}$, let us define a coordinate system t-n where the axes t and n are, respectively, tangent and normal to $\mathcal{C}$ at s (see Fig. 9). For $s=(x_s,y_s)=(n_s,t_s)$, $\phi_{\mathbf{k}}(s)=(2\pi)^{-1}\exp[i(k_xx_s+k_yy_s)]=(2\pi)^{-1}\exp[i(k_tt_s+k_nn_s)]$, with k_t and k_n the components of $\mathbf{k}$ in system t-n. We can think of our potential at s (in the coordinates t-n) as ''separable,'' being a one-dimensional δ function $\gamma_s\delta(n-n_s)$, along n, and zero along t. Thus the term $\exp[ik_tt_s]$ of the incident plane wave $\phi_{\mathbf{k}}$ does not feel the potential. The term $\exp[ik_nn_s]$, however, interacts with the δ potential splitting in two along the n direction. One part is transmitted through $\mathcal{C}$ at s with amplitude $\mathcal{T}$, and the other is reflected from $\mathcal{C}$ at s with amplitude $\mathcal{R}$. Here $\mathcal{T}$ and $\mathcal{R}$ are the transmission and reflection amplitudes for a one-dimensional δ function (see Sec. III B).

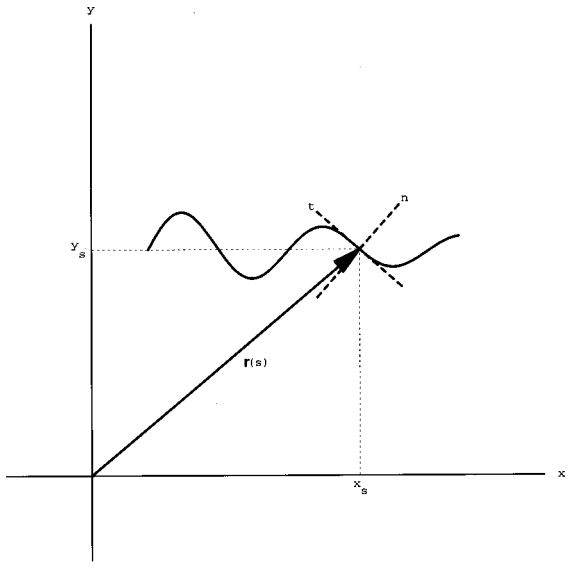

FIG. 9. ''Locally separable'' t-n coordinate system at the point s on $\mathcal{C}$.

When we solve Eq. (2) with $V(\mathbf{r})$ given by Eq. (4), we in fact take into account the scattering of all the components $\phi_{\mathbf{k}}$ of ϕ along all points of $\mathcal{C}$, and then sum these contributions, building up the interference patterns between the incoming and scattered waves.

It is now clear how γ is related to the permeability or transparency of the ''wall'' $\mathcal{C}$. $|\mathcal{T}(k,\gamma(s))|^2$ gives the probability of a plane wave (of wave number k), incident normal to $\mathcal{C}$ at s, to be transmitted through s. The obvious results, $|\mathcal{T}(k,0)|^2=1$ and $|\mathcal{T}(k,+\infty)|^2=0$, follow from the expression for the transmission amplitude in Sec. III B. If $\gamma<0$ the same kind of analysis applies, but then we also have the possibility of bound states on $\mathcal{C}$.

APPENDIX B: GENERAL BOUNDARY CONDITIONS

Handling the general boundary condition (2) is somewhat more difficult than the case of Dirichlet boundary conditions in Sec. II. First, we assume $\mathbf{n}(s)$ a unit vector normal to $\mathcal{C}$ at each point s, and

$$\partial_{\mathbf{n}(s)}f(\mathbf{r}(s))=\mathbf{n}(s)\cdot\nabla f(\mathbf{r}(s)). \tag{B1}$$

Second, we insert Eq. (1) into Eq. (3) to obtain

$$\psi(\mathbf{r})=\phi(\mathbf{r})+\int_{\mathcal{C}}ds'\,\gamma(s')G_0(\mathbf{r},\mathbf{r}(s'))\times\{\alpha(s')-[1-\alpha(s')]\partial_{\mathbf{n}(s')}\}\psi(\mathbf{r}(s')), \tag{B2}$$

which then we consider at a point $\mathbf{r}(s'')$ on $\mathcal{C}$ (with the same notational abbreviation used in Sec. II)

$$\psi(s'')=\phi(s'')+\int ds'\,\gamma(s')G_0(s'',s')\times\{\alpha(s')+[1-\alpha(s')]\partial_{n(s')}\}\psi(s'). \quad \text{(B3)}$$

As it stands, Eq. (B3) is *not* a linear equation in $\psi(s)$. To fix this, we multiply both sides by $\{\alpha(s'')+[1-\alpha(s'')]\partial_{n(s'')}\}$ and define

$$\begin{aligned}\psi^B(s'')&=\{\alpha(s'')+[1-\alpha(s'')]\partial_{n(s'')}\}\psi(s''),\\ \phi^B(s'')&=\{\alpha(s'')+[1-\alpha(s'')]\partial_{n(s'')}\}\phi(s''),\\ G_0^B(s'',s')&=\{\alpha(s'')+[1-\alpha(s'')]\partial_{n(s'')}\}G_0(s'',s').\end{aligned} \quad \text{(B4)}$$

This yields

$$\psi^B(s'')=\phi^B(s'')+\int ds'\,\gamma(s')G_0^B(s'',s')\psi^B(s'), \quad \text{(B5)}$$

which is now a linear equation in ψ^B, and is solved by

$$\tilde{\psi}^B=[\tilde{1}-\tilde{G}_0^B\,\tilde{\Lambda}]^{-1}\tilde{\phi}^B, \quad \text{(B6)}$$

where again the tildes emphasize that the equation is defined only on $\mathcal{C}$. The diagonal operator $\tilde{\Lambda}$ is

$$(\tilde{\Lambda}f)(s)=\gamma(s)f(s). \quad \text{(B7)}$$

We define

$$T^B=\tilde{\Lambda}[\tilde{1}-\tilde{G}_0^B\,\tilde{\Lambda}]^{-1}, \quad \text{(B8)}$$

that solves the original problem

$$\psi(\mathbf{r})=\phi(\mathbf{r})+\int ds'G_0(\mathbf{r},\mathbf{r}(s'))\;T^B_{\phi^B}(\mathbf{r}(s')), \quad \text{(B9)}$$

for

$$T^B_{\phi^B}(\mathbf{r}(s'))=\int ds\;T^B(s',s)\;\phi^B(s). \quad \text{(B10)}$$

As in Sec. II, in the limit $\gamma(s)=\gamma\to\infty$, T^B converges to $-[\tilde{G}_0^B]^{-1}$ which, when inserted into Eq. (B5), gives

$$\{\alpha(s)+[1-\alpha(s)]\partial_{n(s)}\}\psi(s)=\psi^B(s)=([\tilde{1}-\tilde{G}_0^B\,[\tilde{G}_0^B]^{-1}]\tilde{\phi}^B)(s)=0, \quad \text{(B11)}$$

the desired boundary condition (2).

For completeness, we expand T^B in a power series

$$T^B=\tilde{\Lambda}+\tilde{\Lambda}\left(\sum_{j=1}^{\infty}[\tilde{G}_0^B\,\tilde{\Lambda}]^j\right), \quad \text{(B12)}$$

so

$$T^B(s'',s')=\gamma(s'')\;\delta(s''-s')+\gamma(s'')\left(\sum_{j=1}^{\infty}[T^B]^{(j)}(s'',s')\right), \quad \text{(B13)}$$

where

$$[T^B]^{(j)}(s'',s')=\int ds_1\ldots ds_j\;G_0^B(s'',s_j)\times\gamma(s_j)\;\ldots\;G_0^B(s_2,s_1)\gamma(s_1)\delta(s_1-s'), \quad \text{(B14)}$$

allowing one, at least in principle, to compute $T^B(s'',s')$, and thus the wave function everywhere.

[1] M. F. Crommie, C. P. Lutz, and D. M. Eigler, Science **262**, 218 (1993); E. J. Heller, M. F. Crommie, C. P. Lutz, and D. M. Eigler, Nature (London) **369**, 464 (1994).

[2] E. J. Heller, Phys. Rev. Lett. **77**, 4122 (1996).

[3] M. F. Crommie, C. P. Lutz, D. M. Eigler, and E. J. Heller, Physica D **83**, 90 (1995).

[4] M.C. Gutzwiller, *Chaos in Classical and Quantum Mechanics* (Springer-Verlag, New York, 1991).

[5] B. Dietz, J. P. Eckmann, C. A. Pillet, U. Smilansky, and I. Ussishkin, Phys. Rev. E **15**, 4222 (1995).

[6] E. J. Heller, in *Chaos and Quantum Physics*, edited by M. J. Giannoni, A. Voros, and J. Zinn-Justin (Elsevier, Amsterdam, 1990).

[7] F. Hartmann, *Introduction to Boundary Elements: Theory and Applications* (Springer, Berlin, 1989); G.S. Gipson, *Boundary Element Fundamentals* (Computational Mechanics, Southampton, UK, 1987); G. Beer and J.O. Watson, *Introduction to Finite Element and Boundary Element Methods for Engineers* (Wiley, New York, 1992).

[8] R. Goloskie, T. Thio, and L. R. Ram-Mohan, Comput. Phys. **10**, 477 (1996).

[9] Here we will assume a pragmatic point of view by supposing that our mathematical problem is well posed, i.e., that a solution for the Schrödinger equation does exist, satisfying the boundary conditions considered. Obviously, the method has no meaning when this is not so.

[10] C. Grosche, Phys. Rev. Lett. **71**, 1 (1993); Ann. Phys. (Leipzig) **2**, 557 (1993).

[11] L. S. Rodberg and R. B. Thaler, *Introduction to the Quantum Theory of Scattering* (Academic, New York, 1967); M.L. Goldberger and K.M. Watson, *Collision Theory* (Wiley, New York, 1964); D. Lessie and J. Spadaro, Am. J. Phys. **5**, 909 (1985).

[12] G. Arfken, *Mathematical Methods for Physicists* (Academic, New York, 1970).

[13] I.S. Gradshteyn and I.M. Ryzhik, in *Table of Integrals, Series and Products*, edited by Alan Jeffrey (Academic, San Diego, 1994).

[14] C. Grosche, J. Phys. A **23**, 5205 (1990).

[15] This assures a one-to-one map from $\mathcal{C}^B$ to $\mathcal{C}^A$. The distance (the segment's length) between the points labeled s'' and s' on $\mathcal{C}^B$ is the same than the distance between the points also labeled s'' and s' on $\mathcal{C}^A$. Furthermore, $s=0$ and $s=s_{\max}$ correspond, in both curves, to their extreme points. If the $\mathcal{C}$'s are not of the same total length, one can always rescale them.

[16] E. Doron and U. Smilansky, Nonlinearity **5**, 1055 (1992); C. Rouvinez and U. Smilanksy, J. Phys. A **28**, 77 (1995).